

Detection of intrinsic cluster alignments to $100h^{-1}\text{Mpc}$ in the SDSS

A. Smargon¹, R. Mandelbaum^{1,2*}, N. Bahcall¹, M. Niederste-Ostholt³

¹Department of Astrophysical Sciences, Princeton University, Peyton Hall, Princeton, NJ 08544, USA

²Department of Physics, Carnegie Mellon University, Pittsburgh, PA 15213, USA

³Institute of Astronomy, Madingley Rd, Cambridge, CB3 0HA

2 February 2012

ABSTRACT

We measure the large-scale intrinsic alignments of galaxy clusters in the Sloan Digital Sky Survey (SDSS) using subsets of two cluster catalogues: 6625 clusters with $0.1 < z < 0.3$ from the maxBCG cluster catalogue (Koester et al. 2007a, 7500 deg²), and 8081 clusters with $0.08 < z < 0.44$ from the Adaptive Matched Filter catalogue (Dong et al. 2008, 6500 deg²). We search for two types of cluster alignments using pairs of clusters: the alignment between the projected major axes of the clusters ('correlation' alignment), and the alignment between one cluster major axis and the line connecting it to the other cluster in the pair ('pointing' alignment). In each case, we use the cluster member galaxy distribution as a tracer of the cluster shape. All measurements are carried out with each catalogue separately, to check for dependence on cluster selection procedure. We find a strong detection of the pointing alignment on scales up to $100h^{-1}\text{Mpc}$, at the 6 or 10σ level depending on the cluster selection algorithm used. The correlation alignment is only marginally detected up to $\sim 20h^{-1}\text{Mpc}$, at the 2 or 2.5σ level. These results support our current theoretical understanding of galaxy cluster intrinsic alignments in the Λ CDM paradigm, although further work will be needed to understand the impact of cluster selection effects and observational measurement errors on the amplitude of the detection.

Key words: cosmology: observations – large-scale structure of Universe – dark matter – galaxies: clusters: general.

1 INTRODUCTION

The Λ CDM cosmological paradigm features a cosmic web containing galaxies, filaments, galaxy clusters, and larger superclusters. These structures are hosted by dark matter halos which are predicted to have shapes that are aligned with each other due to tidal forces and coherent matter infall along filaments (Croft & Metzler 2000; Heavens et al. 2000; Catelan et al. 2001; Crittenden et al. 2001; Jing 2002; Hopkins et al. 2005). These alignments are manifested in various ways: for example, as alignments of galaxy or galaxy cluster shapes towards overdensities; alignments of pairs of galaxy or cluster shapes with each other; and alignments of galaxy cluster shapes with the shape of the Brightest Cluster Galaxy (BCG).

Recent intrinsic alignments work has focused on galaxies, in part because of the pernicious effects of such alignments on weak lensing measurements (e.g., Croft & Metzler 2000; Hirata & Seljak 2004). This work suggests that the

large-scale ($10\text{--}100h^{-1}\text{ Mpc}$) intrinsic alignments of galaxies are a complex function of luminosity, colour and/or morphological type (e.g., Mandelbaum et al. 2006; Hirata et al. 2007). The non-detection of intrinsic alignments for lower luminosity galaxies ($\lesssim L_*$) may result from misalignment between the galaxy light distribution and the underlying dark matter halo shape (Heymans et al. 2006; Bett 2011).

If we want to measure intrinsic alignments with fewer systematic errors, we might instead consider the projected (2d) intrinsic alignments of galaxy clusters. The cluster member galaxies trace the cluster shape sufficiently well that they should be useful for testing the Λ CDM predictions for intrinsic alignments of cluster-scale dark matter halos (as suggested by a successful stacked weak lensing measurement of cluster ellipticity in the SDSS, Evans & Bridle 2009, which is only feasible if the cluster shape traced by the member galaxies strongly correlates with the shape of the underlying dark matter halo). There are several sets of theoretical predictions (Splinter et al. 1997; Onuora & Thomas 2000; Faltenbacher et al. 2002; Hopkins et al. 2005) that qualitatively agree that cluster intrinsic alignments should extend

* rmandelb@astro.princeton.edu

to $\sim 100h^{-1}$ Mpc scales for a Λ CDM cosmology (though minor disagreements arise due to different N -body simulation volumes, resolutions, and cosmologies). Additional theoretical work has quantified the environment-dependence of such alignments; e.g., Altay et al. (2006) found that the shapes of nearby clusters are aligned if the clusters are connected by a filament. Thus, matter infall along filaments is an important factor in galaxy cluster intrinsic alignments (see also Hopkins et al. 2005).

There were several early attempts to measure intrinsic alignments of galaxy cluster shapes up to tens of Mpc scales (Binggeli 1982; Struble & Peebles 1985; Flin 1987; Lambas et al. 1988; Ulmer et al. 1989; West 1989; Plionis 1994). Typically, they used small, inhomogeneous cluster samples; results were conflicting and the reported detections were typically low in significance, and limited to $\lesssim 30h^{-1}$ Mpc.

Recent work has demonstrated several smaller-scale cluster alignments. For example, alignments of groups within the local supercluster have been demonstrated up to 20 Mpc scales (Godlowski & Flin 2010). Using larger samples, the alignment of the shape of the BCG or the X-ray isophotes with that of the host cluster has been robustly demonstrated (Fuller et al. 1999; Kim et al. 2002; Hashimoto et al. 2008; Niederste-Ostholt et al. 2010; Hao et al. 2011). Moreover, correlations have been detected up to $30h^{-1}$ Mpc between the cluster X-ray isophotes and the position of the nearest neighbour cluster, or the density field traced by spectroscopic galaxy positions (Chambers et al. 2000, 2002; Wang et al. 2009; Paz et al. 2011). Given these promising results with larger, more homogeneous cluster samples, we attempt to detect, for the first time, the intrinsic alignments of galaxy clusters on the largest scales for which there is a theoretical prediction ($100h^{-1}$ Mpc), using SDSS data.

2 DATA

The SDSS (York et al. 2000) imaged roughly π steradians of the sky by drift-scanning the sky in photometric conditions (Hogg et al. 2001; Ivezić et al. 2004) in five bands ($ugriz$; Fukugita et al. 1996; Smith et al. 2002) using a specially-designed wide-field camera (Gunn et al. 1998). The data were processed by automated pipelines that detect and measure photometric properties of objects, and astrometrically calibrate the data (Lupton et al. 2001; Pier et al. 2003; Tucker et al. 2006). This paper relies on SDSS Data Release 6 (DR6, Adelman-McCarthy et al. 2008).

We use two pre-existing catalogues of galaxy clusters based on photometric data. The first is the maxBCG catalogue (Koester et al. 2007a,b), which includes 12 766 clusters in 7500 deg^2 , with $0.1 < z < 0.3$, detected by searching for an overdensity of red galaxies. This catalogue includes clusters with ≥ 10 red sequence member galaxies with $L \geq 0.4L_*$ within the cluster radius R_{200} . The second catalogue (Dong et al. 2008) results from using the Adaptive Matched Filter (AMF) algorithm to identify galaxy overdensities (not necessarily red) over a larger redshift range, yielding 36 785 clusters in 6500 deg^2 , each with ≥ 20 member galaxies with $L \geq 0.4L_*$. Both catalogues have photometric redshifts with typical uncertainty $\Delta z_{\text{phot}} \sim 0.015$, which complicates the identification of nearby cluster pairs. Comparison of results for the two catalogues may indicate how differences in the

cluster selection procedure affect our ability to measure intrinsic alignments.

The analysis requires measurements of the cluster shapes. We use the shapes measured by Niederste-Ostholt et al. (2010), who identified red cluster member galaxies within 0.5 Mpc of the geometric cluster centre, and measured cluster shapes using the radius-weighted second moments of the galaxy distribution. To obtain a sample with reliable shapes, Niederste-Ostholt et al. (2010) recommend a series of cuts on the clusters as shown in Table 1, resulting in final catalogues of 8081 and 6625 clusters with shapes for AMF and maxBCG, respectively. The cut to the redshift range $0.08 < z < 0.44$, which is necessary for robust identification of the red sequence, only affects the AMF catalogue, since the maxBCG catalogue is limited to a narrower redshift range already. One cut, requiring that the cluster ellipticity be inconsistent with zero at $> 1\sigma$, may introduce a potential bias on the systems that are selected. The original reason for this cut is that, for a given number of member galaxies, as the ellipticity appears rounder, the position angle that is estimated becomes noisier. Extremely noisy position angles will wash out an alignment signal that might actually be present if we were able to measure the cluster shape to arbitrary precision.

While we require that ≥ 5 member galaxies are used to determine the shapes, only 5–6 were used for the majority of the clusters¹. The small number of galaxies used to determine shapes may introduce some random noise into the position angles (as in figure 10 of Niederste-Ostholt et al. 2010), which will tend to dilute intrinsic alignment signals.

3 INTRINSIC ALIGNMENTS ESTIMATOR

To begin, we isolate cluster pairs that may be associated (in 3d). For each possible cluster pair, we compute its angular separation on the sky, $\Delta\phi$, and require it to be consistent with a comoving separation of $R \leq 100h^{-1}$ Mpc at the mean photometric redshift of the pair (using a fiducial flat Λ CDM cosmology with $\Omega_m = 0.27$, and expressing our results with $h = 1$). Along the line-of-sight, we require $\Delta z = |z_1 - z_2| \leq 0.015$, a redshift separation corresponding to the 1σ photometric redshift error (the impact of this selection will be discussed in Sec. 5). There are a total of 103 175 and 58 899 cluster pairs for the maxBCG and AMF catalogues, respectively. Each cluster can in principle be included in several cluster pairings.

We divide the cluster pairs into 9 logarithmically spaced bins in R , from 1 to $100h^{-1}$ Mpc. For each pair, we compute two statistics defined in Hopkins et al. (2005): the ‘correlation angle’ θ_c is the angle between the projected major axes of the two clusters, and the ‘pointing angle’ θ_p is the angle on the sky between the projected cluster major axis and the

¹ This ≥ 5 cut used for the determination of shapes may seem inconsistent with the quoted richness thresholds for the AMF and maxBCG cluster catalogues of 20 and 10 cluster members. In fact, the cut used for shape determination is more stringent, both because it requires that the member galaxies be red (unlike the AMF richness estimator) and, more importantly, that they lie within 0.5Mpc of the cluster centre, rather than within the virial radius which may be several times larger.

	AMF clusters	maxBCG clusters
Input catalogue	36 785	12 766
$0.08 < z < 0.44$ (AMF), $0.1 < z < 0.3$ (maxBCG)	23 106	12 766
Geometric centre < 0.5 Mpc from input centre	21 711	12 202
BCG within 0.5 Mpc of geometric centre	14 053	10 754
Inconsistent with being round at $> 1\sigma$	9115	7071
≥ 5 member galaxies used to define shape	8081	6625

Table 1. Cuts imposed on clusters in both cluster catalogues, in order to obtain reliable position angle measurements (from Niederste-Ostholt et al. 2010).

line connecting one cluster to the other cluster in the pair. Thus, θ_c indicates the alignment of the cluster shapes with each other, and θ_p indicates whether clusters tend to point towards other clusters. In each R bin, we compute the mean $\langle \cos^2 \theta_c \rangle$ and likewise for θ_p ; this statistic would be 0.5 for a purely random distribution of cluster shapes.

We estimate errorbars by assigning each cluster a random orientation angle. We then redo the measurement procedure with the random angles, in which case the ideal signal is a known value, $\langle \cos^2 \theta_{c,p} \rangle = 0.5$. Deviations from that value can be used to quantify the noise in $\langle \cos^2 \theta_{c,p} \rangle$ in the real measurement due to the finite number of cluster pairs used for the analysis. The errorbars shown on the plot are the standard deviation of the mean $\cos^2 \theta_{c,p}$.

4 OBSERVATIONAL RESULTS

In this section, we present the results of the measurement described in Sec. 3. Fig. 1 shows the correlation angle alignment for both cluster catalogues. As shown, the correlation angle alignment is detected below $20h^{-1}$ Mpc, but with large error bars, and represents a 2.5σ (AMF) and 2σ (maxBCG) detection summed over these radial bins. The suppressed signal for $R < 3h^{-1}$ Mpc in the AMF catalogue may result from the difficulty in identifying cluster pairs with small separation and measuring their shapes, given that this separation is comparable to the typical cluster size. It is unclear why the maxBCG algorithm seems to do slightly better in this respect.

Fig. 2 shows the measured pointing angle alignments, for which there is clearly a signal on all scales, indicating that clusters tend to point towards other clusters out to $100h^{-1}$ Mpc. This signal is detected at 6σ (AMF) and 10σ (maxBCG) averaged over $1 < R < 100h^{-1}$ Mpc scales, with the detection significance remaining strong beyond $50h^{-1}$ Mpc but dropping to 1σ in the outermost bin.

The errors are smaller for the pointing angle measurement than for the correlation angle (Fig. 1) by roughly a factor of two, for two reasons. First, the correlation angle includes two position angles but the pointing angle includes only one², and so comparatively the errors on the point-

² The pointing angle does have an additional source of statistical error due to uncertainty in the cluster centroid positions, which affects determination of the line connecting the two clusters. However, this form of uncertainty is far less important than the position angle uncertainty when the clusters are separated by R larger than a few cluster virial radii.

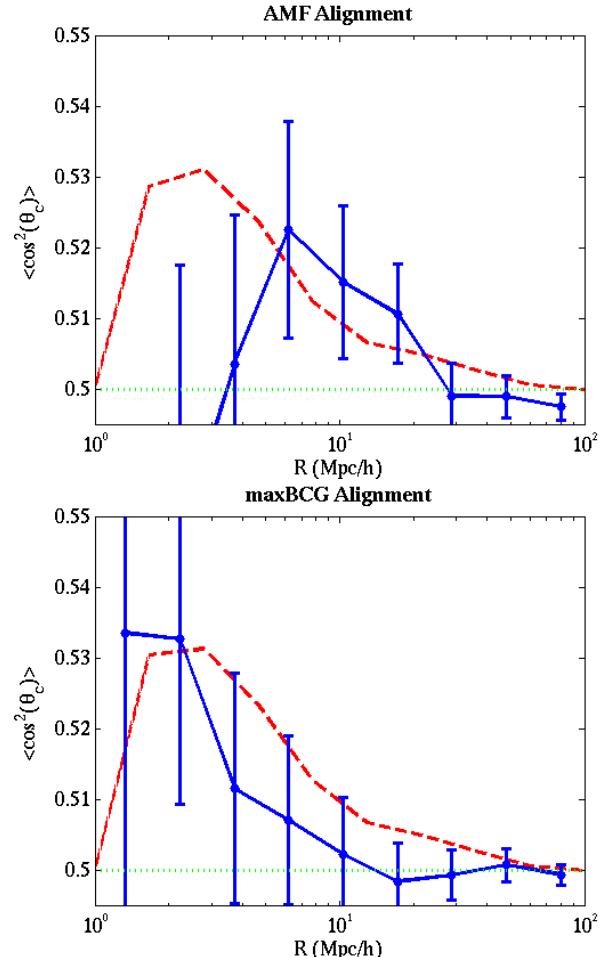


Figure 1. The cluster correlation angle alignment $\langle \cos^2 \theta_c \rangle$, as a function of comoving pair separation R , for AMF (top) and maxBCG (bottom) catalogues. The blue points with errorbars are the observational results (Sec. 4); the red dashed lines are theoretical predictions corrected for photometric redshift uncertainties (Sec. 5); and the green dotted horizontal lines indicate purely random cluster orientations. The errors between the different bins in R are independent.

ing angle alignment are lowered by an initial factor of $\sqrt{2}$. Second, for each cluster pair, there are two pointing angles but only one correlation angle. As a result, each cluster pair contributes twice to the pointing angle measurement, which reduces the errors on it by another factor of $\sqrt{2}$.

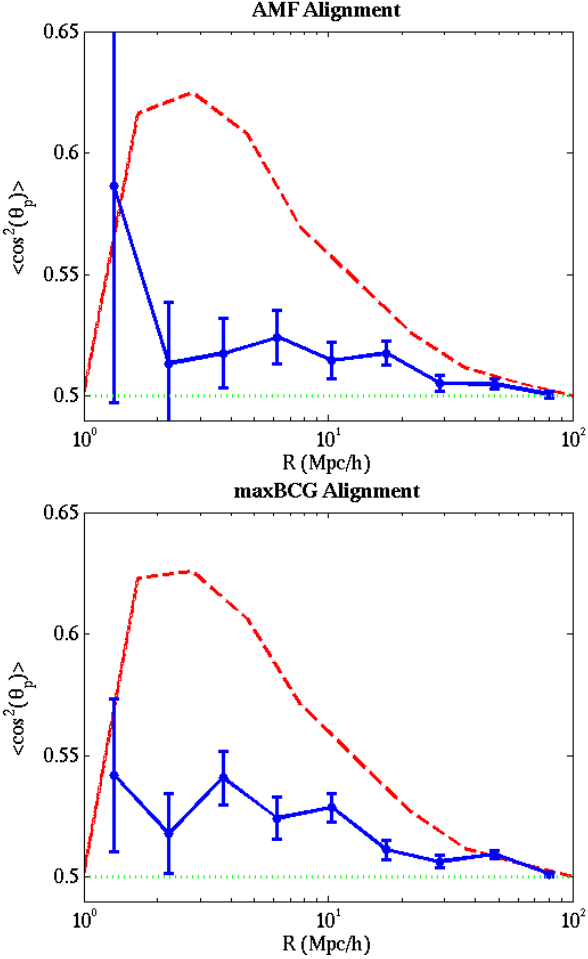


Figure 2. The cluster pointing angle alignment $\langle \cos^2 \theta_p \rangle$, as a function of comoving pair separation R , for AMF (top) and maxBCG (bottom) catalogues. The line format is the same as in Fig. 1.

5 COMPARISON WITH THEORY

We compare these observations with the theoretical predictions for a Λ CDM cosmology from Hopkins et al. (2005). That study utilised a 2×10^9 particle N -body simulation to study the evolution of cluster ellipticity, orientation, and alignment for $0 < z < 3$. The simulation box length was $1500h^{-1}$ Mpc, resulting in a large simulated cluster sample. The force softening length was $17h^{-1}$ kpc, so the spatial resolution was more than sufficient to resolve the cluster halos. Only masses above $2 \times 10^{13}h^{-1}M_\odot$ were considered as clusters.

The observations include many systematic errors that are not in the simulation. The most important ones are (1) the line-of-sight redshift selection and complications due to photometric redshift error, (2) cluster centroiding error (misidentification of the BCG due to some algorithmic error), (3) noise in the determination of the cluster position angle due the small number of cluster member galaxies (≥ 5) used to estimate the cluster shape, and (4) the need to exclude clusters that appeared nearly round, due to the difficulty in estimating a position angle. The first three of these systematic errors will reduce our ability to detect intrinsic

alignments and weaken the observed signal. Thus, we do not compare with the direct predictions of Hopkins et al. (2005) (for their $0 < z < 0.5$ sample), but rather with reduced predictions as described below.

The line-of-sight pair selection criterion, $|\Delta z_{\text{phot}}| < 0.015$, was chosen to balance competing considerations. In the absence of photometric redshift error, we would ideally attempt to mimic the Hopkins et al. (2005) selection of pairs within $100h^{-1}$ Mpc; even with spectroscopic redshifts this would be complicated by redshift-space distortions, but we could at least hope to come fairly close to what was done in the simulations. However, the photometric redshift errors correspond to typical separations of $\sim 50h^{-1}$ Mpc, making it impossible to imitate a strict line-of-sight separation. We could simply choose a Δz corresponding roughly to $100h^{-1}$ Mpc, but empirical tests showed that the contamination from completely unassociated clusters along the line-of-sight became unacceptably large. These unassociated clusters dilute the expected signal and therefore the detection significance since their orientations are purely random, and indeed, even with our chosen Δz_{phot} , we must impose a correction for it (to be described below). We therefore err on the conservative side and use a Δz_{phot} corresponding to roughly the 1σ photometric redshift error in order to be able to measure the signal.

The contamination due to accidental inclusion of unassociated clusters because of photometric redshift error can be estimated via simulation. We simulate galaxy clusters with constant comoving number density, assign a photo- z assuming $\sigma(z_{\text{phot}}) = 0.015$ (Gaussian), and estimate what fraction of the clusters within $|\Delta z_{\text{phot}}| = 0.015$ are actually $> 100h^{-1}$ Mpc apart on the line-of-sight (with this separation chosen because it is the criterion used by Hopkins et al. 2005). Given a contamination fraction $0 < \Gamma < 1$ defined as the fraction of cluster pair candidates that satisfy our $|\Delta z_{\text{phot}}|$ cut but that are more than $100h^{-1}$ Mpc apart along the line-of-sight, and theoretical predictions $\langle \cos^2 \theta_{c,p} \rangle_{\Lambda\text{CDM}}$, we compare our measured signals with

$$\langle \cos^2 \theta_{c,p} \rangle_{\text{smeared}} = 0.5\Gamma + (1 - \Gamma)\langle \cos^2 \theta_{c,p} \rangle_{\Lambda\text{CDM}}. \quad (1)$$

We cannot estimate Γ from the random, simulated clusters alone, because that simulation only tells us the relative contamination when the intrinsic (3d) cluster correlation function $\xi \ll 1$. When clustering is significant, the relative contamination becomes smaller. We quantify this effect by using the simulated contamination fraction $\beta = 0.35$ in the absence of clustering, and the observed (projected) cluster correlation function. The simulated contamination fraction can be defined $\beta = N_S/(N_S + N_R)$ where N_S represents spurious cluster pairs that appear within our Δz_{phot} due only to photometric redshift error, and N_R represents those real pairs that are expected due to a purely random distribution of clusters in the survey volume. What we really care about is $\Gamma = N_S/(N_S + N_R + N_E)$ where N_E represents the excess cluster pairs that are there in reality due to a non-zero cluster correlation function. Fortunately, we also measure the projected correlation function,

$$\begin{aligned} w(R) + 1 &= \frac{N_{\text{pairs}} \text{ in real data}}{N_{\text{pairs}} \text{ in random cluster catalogue}} \\ &= \frac{N_R + N_S + N_E}{N_R + N_S}. \end{aligned} \quad (2)$$

To estimate Γ we then use

$$\Gamma(R) = \frac{\beta}{1 + w(R)}. \quad (3)$$

In the case that clustering is insignificant, as on large scales, $w \approx 0$ and $\Gamma(R) = \beta = 0.35$. On the smallest scales, we find $w \approx 2$ and therefore $\Gamma \approx 0.12$. This calculation assumes a Gaussian photo- z error distribution, which is unlikely to be valid in detail. Large tails in the photo- z error distribution would tend to further weaken the observed signal.

The theoretical predictions shown in Figs. 1 and 2 have been multiplied by this scale-dependent correction factor for photometric redshift error. Still, the observed signals (especially the pointing angle alignment) are weaker than the theoretical predictions, even accounting for this contamination. The correlation alignment is marginally consistent with the theoretical predictions. For the pointing angle, while the alignments are strongly detected ($\sim 10\sigma$), they are considerably weaker than the theoretical predictions.

The effect of the second observational error considered here, cluster centroiding error, is more difficult to model accurately. While maxBCG centroiding errors have been modeled on mock catalogues (Johnston et al. 2007), realistic cluster centroiding errors have only been estimated for special cluster subsamples such as the very massive ones that have strong X-ray detections (e.g., Ho et al. 2009). Thus, modeling this effect is beyond the scope of this paper, and we merely state that it should reduce the observed correlations.

Third, we estimate the impact of computing the cluster ellipticity and position angle from only ≥ 5 (typically 5–6) galaxies. In principle, this introduces measurement error in the position angles that is typically 15 degrees (Niederste-Ostholt et al. 2010), which will dilute the predicted signal (it also increases the noise, but we have correctly accounted for this in our estimation of errorbars already). While the effect of statistical error in the cluster position angles is in principle complicated, we can appeal to simple arguments to roughly estimate its impact. It should result in the true distribution of correlation or pointing angles, $p(\cos^2 \theta_{c,p})$, being convolved with some error distribution, which we assume to be Gaussian. Unfortunately, Hopkins et al. (2005) do not report a full distribution of $\cos^2 \theta_{c,p}$, only its mean value. Thus, to estimate the effect on our statistic $\langle \cos^2 \theta_{c,p} \rangle$, we arbitrarily assume that $p(\cos^2 \theta_{c,p}) = A + B \cos^2 \theta_{c,p}$. We fix the values of A and B by imposing two requirements: that the probability distribution be normalised to 1, and that $\langle \cos^2 \theta_{c,p} \rangle$ should be consistent with the simulations. Then, we convolve that distribution with a Gaussian distribution with $\sigma_{\text{obs},c,p}$ (where $\sigma_{\text{obs},c} = \sqrt{2}\sigma_{\text{obs},p}$ since the former includes two position angles and the latter includes one). In this simple limit, for small $\sigma_{\text{obs},c,p}$, we expect an observed correlation

$$\langle \cos^2 \theta_{c,p} \rangle_{\text{obs}} = 0.5 + e^{-2\sigma_{\text{obs},c,p}^2} [\langle \cos^2 \theta_{c,p} \rangle - 0.5]. \quad (4)$$

This reduces to $\langle \cos^2 \theta \rangle_{\text{obs}} = \langle \cos^2 \theta \rangle$ as $\sigma_{\text{obs},c,p}$ approaches zero. Following Niederste-Ostholt et al. (2010), if we assume that the position angle errors are typically ~ 15 deg, then the correlations are reduced by ~ 15 per cent. This reduction cannot account for the apparent difference between theory and observation in Fig. 2, which means that reconciling this detection with the theory will require more detailed modeling of observational systematic errors.

Finally, we consider the impact of excluding those clusters that are within 1σ of being round and therefore have poorly defined position angles. There are two options to consider. The first is that those clusters truly are round (typically cluster dark matter halos are triaxial in N -body simulations, but could appear nearly round due to projection at certain position angles). In that case, the theoretical predictions for the pointing and correlation angle statistics include a contribution of zero from such round clusters, and our exclusion of them will artificially inflate the signal. The second option is that the clusters are not round, but that they appear so due to noise given that typically only 5–6 galaxies are used to define the shape; this option likely represents the majority of the clusters that were excluded. In that case, the theoretical predictions include some real alignment signal for these clusters, which cannot be measured in reality since their position angles are too noisy. If we were to include them, it would dilute the measured signal. Excluding them is the proper choice in this case, and as long as those clusters that are excluded are a representative subsample with respect to intrinsic alignment properties, then it should not cause any bias in the signal. Nonetheless, future work should include a more careful simulation with such effects directly incorporated before generating theoretical predictions.

6 DISCUSSION

In this paper, we have presented a strong detection of galaxy cluster intrinsic alignments to very large scales of $100h^{-1}\text{Mpc}$, representing a tendency of clusters to point preferentially towards other clusters. Depending on the method used to select clusters and assign photometric redshifts, the strength of the detection (averaged over $1 < R < 100h^{-1}\text{Mpc}$) ranges from 6σ to 10σ . The alignment of pairs of cluster position angles with each other was only detected at the $2\text{--}2.5\sigma$ level. This measurement constitutes the first strong detection of the intrinsic alignments of clusters to $100h^{-1}\text{Mpc}$ with a large, statistical cluster sample ($6\text{--}8 \times 10^3$ clusters) using a uniform set of photometric data.

The observed correlation angle alignment is consistent, within the large error bars, with the theoretical ΛCDM prediction. The pointing angle alignment, while strongly detected to $100h^{-1}\text{Mpc}$, is weaker than expected; this is likely due to various systematic observational uncertainties, all of which tend to weaken the observed signal. We find that photometric redshift error cannot fully account for the dilution of the signal. Future work may include an exploration of how the signal varies with the BCG dominance, to test whether merging clusters might be responsible for diluting the alignment signal. It would also be helpful to carry out this measurement using a sample spanning a broader redshift range, to check for redshift evolution. These future investigations can be used to understand the primary source of the alignments, i.e. whether they are primordial or due to tidal torques from the large-scale density field that would lead to an increase at later times.

A more detailed comparison of these observations with ΛCDM would require simulations that fully incorporate cluster selection effects (including false cluster identification, incorrect division of larger clusters into two smaller clusters, etc.), centroiding errors, the shape estimation procedure in-

cluding the elimination of round clusters, and position angle uncertainties. This level of detail is beyond the scope of this work. However, we have demonstrated the power of large imaging surveys such as SDSS to detect for the first time the cluster intrinsic alignments to very large scales of $100h^{-1}\text{Mpc}$, which can test the ΛCDM prediction of massive dark matter halo alignments. This finding suggests that large imaging surveys planned for the near future, and eventually the Large Synoptic Survey Telescope (LSST), should be successful in mapping out cluster intrinsic alignments as a function of cluster mass and redshift.

ACKNOWLEDGMENTS

The authors would like to thank the anonymous referee for constructive feedback that led to improvements in the quality of this work. We thank Michael Strauss for providing useful comments about this project.

REFERENCES

Adelman-McCarthy J. K. et al., 2008, ApJS, 175, 297
 Altay G., Colberg J. M., Croft R. A. C., 2006, MNRAS, 370, 1422
 Bett P. E., 2011, preprint (arXiv:1108.3717)
 Binggeli B., 1982, A&A, 107, 338
 Catelan P., Kamionkowski M., Blandford R. D., 2001, MNRAS, 320, L7
 Chambers S. W., Melott A. L., Miller C. J., 2000, ApJ, 544, 104
 Chambers S. W., Melott A. L., Miller C. J., 2002, ApJ, 565, 849
 Crittenden R. G., Natarajan P., Pen U., Theuns T., 2001, ApJ, 559, 552
 Croft R. A. C., Metzler C. A., 2000, ApJ, 545, 561
 Dong F., Pierpaoli E., Gunn J. E., Wechsler R. H., 2008, ApJ, 676, 868
 Evans A. K. D., Bridle S., 2009, ApJ, 695, 1446
 Faltenbacher A., Gottlöber S., Kerscher M., Müller V., 2002, A&A, 395, 1
 Flin P., 1987, MNRAS, 228, 941
 Fukugita M., Ichikawa T., Gunn J. E., Doi M., Shimasaku K., Schneider D. P., 1996, AJ, 111, 1748
 Fuller T. M., West M. J., Bridges T. J., 1999, ApJ, 519, 22
 Godłowski W., Flin, P., 2010, ApJ, 708, 920
 Gunn J. et al., 1998, AJ, 116, 3040
 Hao J., Kubo J. M., Feldmann R., Annis J., Johnston D. E., Lin H., McKay T. A., 2011, ApJ, 740, 39
 Hashimoto Y., Henry J. P., Boehringer H., 2008, MNRAS, 390, 1562
 Heavens A., Refregier A., Heymans C., 2000, MNRAS, 319, 649
 Heymans C., White M., Heavens A., Vale C., van Waerbeke L., 2006, MNRAS, 371, 750
 Hirata C. M., Mandelbaum R., Ishak M., Seljak U., Nichol R., Pimbblet K. A., Ross N. P., Wake D., 2007, MNRAS, 381, 1197
 Hirata C. M., Seljak U., 2004, Phys.Rev.D, 70, 063526
 Ho S., Lin Y.-T., Spergel D., Hirata C. M., 2009, ApJ, 697, 1358
 Hogg D. W., Finkbeiner D. P., Schlegel D. J., Gunn J. E., 2001, AJ, 122, 2129
 Hopkins P. F., Bahcall N. A., Bode P., 2005, ApJ, 618, 1
 Ivezić Ž. et al., 2004, Astron. Nachr., 325, 583
 Jing Y. P., 2002, MNRAS, 335, L89
 Johnston D. E. et al., 2007, preprint (arXiv:0709.1159)
 Kim R. S. J., Annis J., Strauss M. A., Lupton R. H., 2002, in ASP Conf. Ser. 268: Tracing Cosmic Evolution with Galaxy Clusters, 395
 Koester B. P., McKay T. A., Annis J., Wechsler R. H., Evrard A. E., Rozo E., Bleem L., Sheldon E. S., Johnston D., 2007a, ApJ, 660, 221
 Koester B. P. et al., 2007b, ApJ, 660, 239
 Lambas D. G., Groth E. J., Peebles P. J. E., 1988, AJ, 95, 996
 Lupton R. H., Gunn J. E., Ivezić Ž., Knapp G. R., Kent S., Yasuda N., 2001, in ASP Conf. Ser. 238: Astronomical Data Analysis Software and Systems X, 269
 Mandelbaum R., Hirata C. M., Ishak M., Seljak U., Brinkmann J., 2006, MNRAS, 367, 611
 Niederste-Ostholt M., Strauss M. A., Dong F., Koester B. P., McKay T. A., 2010, MNRAS, 405, 2023
 Onuora L. I., Thomas P. A., 2000, MNRAS, 319, 614
 Paz D. J., Sgró M. A., Merchán M., Padilla N., 2011, MNRAS, 414, 2029
 Pier J. R., Munn J. A., Hindsley R. B., Hennessy G. S., Kent S. M., Lupton R. H., Ivezić Ž., 2003, AJ, 125, 1559
 Plionis M., 1994, ApJS, 95, 401
 Smith J. et al., 2002, AJ, 123, 2121
 Splinter R. J., Melott A. L., Linn A. M., Buck C., Tinker J., 1997, ApJ, 479, 632
 Struble M. F., Peebles P. J. E., 1985, AJ, 90, 582
 Tucker D. et al., 2006, Astron. Nachr., 327, 821
 Ulmer M. P., McMillan S. L. W., Kowalski M. P., 1989, ApJ, 338, 711
 Wang Y., Park C., Yang X., Choi Y.-Y., Chen X., 2009, ApJ, 703, 951
 West M. J., 1989, ApJ, 344, 535
 York D. et al., 2000, AJ, 120, 1579